Thrust and Torque Vector Characteristics of Axially-Symmetric E-Sail

Marco Bassetto, Giovanni Mengali, Alessandro A. Quarta*

Department of Civil and Industrial Engineering, University of Pisa, I-56122 Pisa, Italy

Abstract

The Electric Solar Wind Sail is an innovative propulsion system concept that gains propulsive acceleration from the interaction with charged particles released by the Sun. The aim of this paper is to obtain analytical expressions for the thrust and torque vectors of a spinning sail of given shape. Under the only assumption that each tether belongs to a plane containing the spacecraft spin axis, a general analytical relation is found for the thrust and torque vectors as a function of the spacecraft attitude relative to an orbital reference frame. The results are then applied to the noteworthy situation of a Sun-facing sail, that is, when the spacecraft spin axis is aligned with the Sun-spacecraft line, which approximatively coincides with the solar wind direction. In that case, the paper discusses the equilibrium shape of the generic conducting tether as a function of the sail geometry and the spin rate, using both a numerical and an analytical (approximate) approach. As a result, the structural characteristics of the conducting tether are related to the spacecraft geometric parameters.

Keywords: Electric solar wind sail, thrust and torque model, Sun-facing sail, sail equilibrium shape

Nomenclature

$\mathcal{A}$, $\mathcal{B}$, $\mathcal{C}$, $\mathcal{D}$	=	components of the total force, see Eq. (23), [N]
b	=	dimensionless (shape) coefficient
$\boldsymbol{d}$	=	position vector of ds, [m]
$\mathcal{E}$, $\mathcal{F}$, $\mathcal{G}$	=	components of the total torque, see Eq. (32), [N m]
f	=	distance of ds from (x, y) plane, [m]
$\boldsymbol{F}$	=	total force, with $\|\|\boldsymbol{F}\|\| \triangleq F$, [N]
h	=	dimensionless abscissa
$\hat{\boldsymbol{i}}$	=	unit vector of x-axis
$\hat{\boldsymbol{i}}_k$	=	unit vector of x_k-axis
$\hat{\boldsymbol{j}}$	=	unit vector of y-axis
$\hat{\boldsymbol{k}}$	=	unit vector of z-axis
K	=	dimensionless shaping parameter, see Eq. (58)
L	=	tether length, [m]
m_p	=	proton mass, [kg]
n	=	solar wind number density, [m^{-3}]
$\hat{\boldsymbol{n}}$	=	spin velocity unit vector
N	=	number of tethers
$\hat{\boldsymbol{r}}$	=	Sun-spacecraft unit vector
s	=	curvilinear abscissa, [m]

*Corresponding author

Email addresses: marco.bassetto@ing.unipi.it (Marco Bassetto), g.mengali@ing.unipi.it (Giovanni Mengali), a.quarta@ing.unipi.it (Alessandro A. Quarta)

Published in Acta Astronautica, Vol. 146 May 2018, pp. 134–143. doi: http://dx.doi.org/10.1016/j.actaastro.2018.02.035

S	=	spacecraft center-of-mass
$\hat{\boldsymbol{s}}$	=	unit vector tangent to the tether
$\boldsymbol{T}$	=	total torque, $[\,\mathrm{N\,m}]$
$\boldsymbol{u}$	=	solar wind relative velocity vector, with $\|\|\boldsymbol{u}\|\| \triangleq u$, $[\,\mathrm{m\,s^{-1}}]$
V	=	tether electric potential [V]
V_w	=	solar wind ions electric potential, [V]
(x, y, z)	=	axes of the body reference frame
α_n	=	pitch angle, [rad]
β	=	aperture angle of the right circular cone, [rad]
δ_n	=	clock angle, [rad]
ϵ_0	=	vacuum permittivity, $[\,\mathrm{F\,m^{-1}}]$
ζ_k	=	angle between planes $(\hat{\boldsymbol{i}}_k,\, \hat{\boldsymbol{n}})$ and $(\hat{\boldsymbol{i}},\, \hat{\boldsymbol{n}})$, [rad]
ρ	=	tether linear mass density, $[\,\mathrm{kg\,m^{-1}}]$
σ	=	constant, see Eq. (10), $[\,\mathrm{kg\,m^{-1}\,s^{-1}}]$
τ	=	tether tension force, [N]
$\boldsymbol{\omega}$	=	spacecraft spin velocity, with $\|\|\boldsymbol{\omega}\|\| \triangleq \omega$, $[\,\mathrm{s^{-1}}]$

Subscripts

c	=	conic
k	=	generic tether
l	=	logarithmic
max	=	maximum
p	=	parabolic
r	=	root
s	=	due to solar wind flux
t	=	tip
ω	=	centrifugal

Superscripts

$'$	=	derivative with respect to x

1. Introduction

The Electric Solar Wind Sail (E-sail) is an innovative propulsion system that exploits the solar wind particle momentum to generate a propulsive acceleration in the interplanetary space [1]. The incoming ions interact with an artificial electric field generated on board by means of an electron emitter, which charges a grid of long tethers at a high voltage level, on the order of some tens of kilovolts [2]. The tethers are deployed and maintained stretched by spinning the spacecraft and, in a simplified model, they can be assumed to belong to the same plane orthogonal to the spin axis [3, 4], see Fig. 1. Along with the more classical solar sail, the E-Sail is one of the most promising propellantless propulsion systems, even though it needs electric power to produce the required electric field. Unlike a solar sail, whose propulsive force varies as the inverse square distance from the Sun, a very interesting property of an E-sail is that its maximum thrust modulus is inversely proportional to the heliocentric distance [5].

A non-negligible portion of the current research is intended for investigating how the geometric features of such a propulsion system may affect its in-flight performance in terms of thrust and torque vectors [6, 7, 8]. However, the E-sail propulsive characteristics are quite complex to model, as the thrust (or torque) vector and the sail shape are mutually affected by each other. To get preliminary simulation results, the thrust vector is often modelled through the simplified assumption of a sail shape resembling that of a rigid disc of given radius [9, 10, 11, 12, 13]. In some cases such an approximation may be inaccurate, as the actual shape of each tether depends on the combined effects of the centrifugal force and the solar wind dynamic pressure acting on it. Moreover, it is known that the actual geometric characteristics of the sail shape may significantly affect the performance of an E-sail-based spacecraft. Nevertheless, in a preliminary phase of mission design the mathematical model adopted to describe the sail shape must be simple enough to be successfully implemented

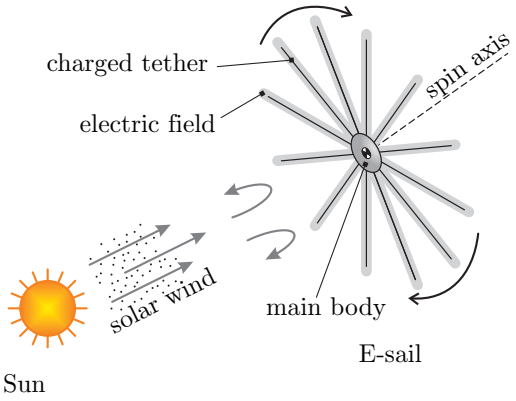

Figure 1: Spinning E-sail conceptual sketch.

within a simulation code, especially when optimal trajectories are investigated [14, 15]. Indeed, in the latter case, a number of transfer trajectories need to be simulated to minimize a scalar performance index, such as the flight time [16, 17, 18, 19].

In this context, Toivanen and Janhunen [8] have studied the shape of a rotating E-sail using a numerical approach, stating that the tether arrangement forms a cone near the spacecraft, while each tether is flattened near the tip by the centrifugal force. More recently, Huo et al. [20] have obtained a compact and analytical description of the E-sail thrust vector using a geometric approach and assuming an axisymmetric grid of tethers belonging to the same plane (the so-called "flat case"). The aim of this paper is to obtain an analytical expression of both thrust and torque vectors generated by a spinning E-sail of a given (three-dimensional) shape, under the main assumption that each tether belongs to a plane containing the spacecraft spin axis. The analytical results are then applied to the noteworthy case of a Sun-facing spinning E-sail [21, 22], thus obtaining a set of analytical (compact) relations.

The problem of describing the actual E-sail equilibrium shape has indeed a substantial simplification when the spacecraft spin axis is aligned with the solar wind velocity vector, the latter being nearly parallel to the Sun-spacecraft direction, see Fig. 2. In that case each tether can be thought of as being aligned with the force field and belonging to a plane containing the spacecraft spin axis. In particular, this paper shows that an approximate, analytical, solution to the E-sail equilibrium shape may be found under the assumption of cylindrical symmetry, that is, when all tethers are the same angle apart from each other. The corresponding tether equilibrium shape is accurately described by a logarithmic arc whose geometric characteristics are related (in an analytical form) to the combined effects of centrifugal and solar wind-induced forces. This result is consistent with the numerical simulations discussed by Toivanen and Janhunen [8]. As such, the new mathematical relations represent an useful improvement over existing models, as they allow the influence of tether arrangement on the propulsion system performance to be quantified without the use of numerical algorithms.

The paper is organized as follows. The resultant force and torque vectors acting on an E-sail of given shape are firstly analyzed in analytical form, starting from the mathematical model discussed in Ref. [2]. The obtained equations are then applied to the important case of a Sun-facing, axially symmetric, E-sail. The approximate form of the tether equilibrium shape is then analytically derived, and the resultant root force is calculated as a function of the tether geometric characteristics and the spacecraft spin rate. Finally, some concluding remarks are given in the last section.

2. Mathematical description of E-sail thrust and torque

Consider an E-sail-based spacecraft that spins about a body-fixed axis with unit vector $\hat{\boldsymbol{n}}$ at an angular velocity $\boldsymbol{\omega} = \omega\,\hat{\boldsymbol{n}}$ of constant modulus ω. The E-sail propulsion system consists of $N \geq 2$ tethers, each one being modelled as a planar cable belonging to the plane $(\hat{\boldsymbol{i}}_k, \hat{\boldsymbol{n}})$, where $\hat{\boldsymbol{i}}_k$ (with $k \in \{0, 1, \ldots, N-1\}$) is a unit vector orthogonal to $\hat{\boldsymbol{n}}$, see Fig. 3.

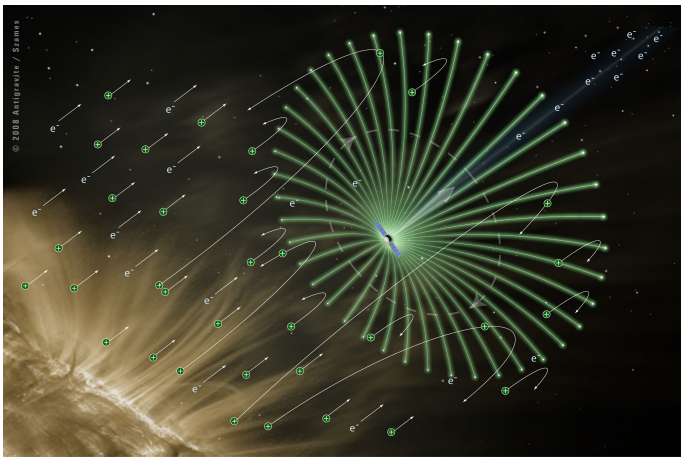

Figure 2: Electric solar wind sail artistic impression. Courtesy of Alexandre Szames, Antigravite (Paris).

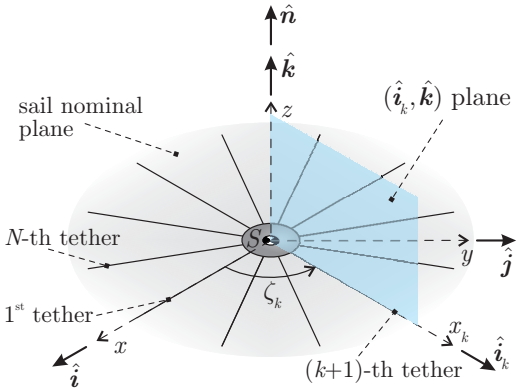

Figure 3: E-sail geometric arrangement.

The displacement of the generic tether with respect to the spacecraft main body can be evaluated by introducing a body reference frame $\mathcal{T}(S; x, y, z)$ with origin S at the spacecraft center-of-mass, and unit vectors $\{\hat{\boldsymbol{i}}, \hat{\boldsymbol{j}}, \hat{\boldsymbol{k}}\}$ defined as

$$\hat{\boldsymbol{k}} \triangleq \hat{\boldsymbol{n}} \quad , \quad \hat{\boldsymbol{i}} \triangleq \hat{\boldsymbol{i}}_0 \quad , \quad \hat{\boldsymbol{j}} \triangleq \hat{\boldsymbol{n}} \times \hat{\boldsymbol{i}}_0 \tag{1}$$

Note that the plane $(\hat{\boldsymbol{i}}, \hat{\boldsymbol{k}})$ contains the first tether, labelled with $k = 0$, whereas the unit vector $\hat{\boldsymbol{i}}_k$ can be written as

$$\hat{\boldsymbol{i}}_k = \cos\zeta_k \, \hat{\boldsymbol{i}} + \sin\zeta_k \, \hat{\boldsymbol{j}} \tag{2}$$

where ζ_k is the angle, measured counterclockwise from the direction of $\hat{\boldsymbol{i}}$, between the x-axis and the x_k-axis with unit vector $\hat{\boldsymbol{i}}_k$, see Fig. 3. In other words, ζ_k is the angle between planes $(\hat{\boldsymbol{i}}, \hat{\boldsymbol{k}})$ and $(\hat{\boldsymbol{i}}_k, \hat{\boldsymbol{k}})$, that is, the planes that contain the first and the $(k+1)$-th tether, respectively.

2.1. E-sail shape model

Assume that the shape of the generic tether can be described, in the plane $(\hat{\boldsymbol{i}}_k, \hat{\boldsymbol{k}})$, through a continuously differentiable function $f_k = f_k(x_k) : [x_{r_k}, x_{t_k}] \to \mathbb{R}$, where $x_{r_k} \geq 0$ (or x_{t_k}) is the distance of the tether root (or tip) from the spacecraft spin axis z, see Fig. 4. The position vector $\boldsymbol{d}_k$ of a generic infinitesimal arc-length $\mathrm{d}s_k$ of the conducting tether is given by

$$\boldsymbol{d}_k = x_k \, \hat{\boldsymbol{i}}_k + f_k \, \hat{\boldsymbol{k}} \tag{3}$$

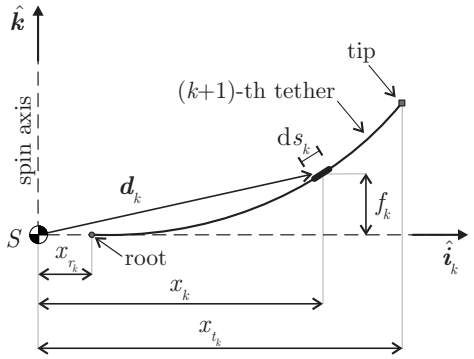

Figure 4: Generic tether displacement.

with

$$\mathrm{d}s_k = \sqrt{1 + (f_k')^2}\,\mathrm{d}x_k \tag{4}$$

where $f_k' \triangleq \mathrm{d}f_k/\mathrm{d}x_k$. From Eqs. (3)-(4), the expression of the (local) unit vector $\hat{\boldsymbol{s}}_k$ tangent to the generic tether at point $(x_k,\, f_k)$ is

$$\hat{\boldsymbol{s}}_k \triangleq \frac{\mathrm{d}\boldsymbol{d}_k}{\mathrm{d}s_k} = \frac{\mathrm{d}x_k\,\hat{\boldsymbol{i}}_k + \mathrm{d}f_k\,\hat{\boldsymbol{k}}}{\sqrt{1 + (f_k')^2}\,\mathrm{d}x_k} \equiv \frac{\hat{\boldsymbol{i}}_k + f_k'\,\hat{\boldsymbol{k}}}{\sqrt{1 + (f_k')^2}} \tag{5}$$

which can be rewritten, using Eq. (2), as a function of $\{\hat{\boldsymbol{i}},\, \hat{\boldsymbol{j}},\, \hat{\boldsymbol{k}}\}$ as

$$\hat{\boldsymbol{s}}_k = \frac{\cos\zeta_k\,\hat{\boldsymbol{i}} + \sin\zeta_k\,\hat{\boldsymbol{j}} + f_k'\,\hat{\boldsymbol{k}}}{\sqrt{1 + (f_k')^2}} \tag{6}$$

2.2. Force acting on tethers

The total force $\mathrm{d}\boldsymbol{F}_k$ acting on the infinitesimal arc-length $\mathrm{d}s_k$ is the sum of the centrifugal force $\mathrm{d}\boldsymbol{F}_{\omega_k}$, and that arising from the solar wind dynamic pressure $\mathrm{d}\boldsymbol{F}_{s_k}$, viz.

$$\mathrm{d}\boldsymbol{F}_k = \mathrm{d}\boldsymbol{F}_{\omega_k} + \mathrm{d}\boldsymbol{F}_{s_k} \tag{7}$$

Recalling that x_k is the distance of $\mathrm{d}s_k$ from the spacecraft spin axis z, the term $\mathrm{d}\boldsymbol{F}_{\omega_k}$ can be written as

$$\mathrm{d}\boldsymbol{F}_{\omega_k} = \rho\,\mathrm{d}s_k\,x_k\,\omega^2\,\hat{\boldsymbol{i}}_k \equiv \rho\,\mathrm{d}s_k\,x_k\,\omega^2\,\left(\cos\zeta_k\,\hat{\boldsymbol{i}} + \sin\zeta_k\,\hat{\boldsymbol{j}}\right) \tag{8}$$

where ρ is the tether (linear) uniform mass density, and $\hat{\boldsymbol{i}}_k$ is given by Eq. (2) as a function of $\{\hat{\boldsymbol{i}},\, \hat{\boldsymbol{j}}\}$. Also, according to the recent works of Janhunen and Toivanen [3, 6, 8], the thrust $\mathrm{d}\boldsymbol{F}_{s_k}$ gained by $\mathrm{d}s_k$, when the Sun-spacecraft distance is on the order of 1 au, is given by

$$\mathrm{d}\boldsymbol{F}_{s_k} = \sigma_k\,\boldsymbol{u}_{\perp k}\,\mathrm{d}s_k \tag{9}$$

with

$$\sigma_k \triangleq 0.18\,\max(0,\, V_k - V_w)\,\sqrt{\epsilon_0\,m_p\,n} \tag{10}$$

where V_k is the tether voltage (on the order of 20–40 kV), V_w is the electric potential corresponding to the kinetic energy of the solar wind ions (with a typical value of about 1 kV), ϵ_0 is the vacuum permittivity, m_p is the solar wind ion (proton) mass, n is the local solar wind number density, and $\boldsymbol{u}_{\perp k}$ is the component of the solar wind velocity $\boldsymbol{u}$ perpendicular to the direction of $\hat{\boldsymbol{s}}_k$ given by Eq. (5).

Assuming a purely radial solar wind stream, that is, $\boldsymbol{u} = u\,\hat{\boldsymbol{r}}$ where $\hat{\boldsymbol{r}}$ is the Sun-spacecraft unit vector and u is the solar wind velocity modulus, the term $\boldsymbol{u}_{\perp k}$ in Eq. (9) is given by

$$\boldsymbol{u}_{\perp k} = u\,(\hat{\boldsymbol{s}}_k \times \hat{\boldsymbol{r}}) \times \hat{\boldsymbol{s}}_k \equiv u\,[\hat{\boldsymbol{r}} - (\hat{\boldsymbol{r}} \cdot \hat{\boldsymbol{s}}_k)\,\hat{\boldsymbol{s}}_k] \tag{11}$$

In particular, according to Fig. 5, the Sun-spacecraft unit vector $\hat{\boldsymbol{r}}$ can be written as a function of $\{\hat{\boldsymbol{\imath}},\, \hat{\boldsymbol{\jmath}},\, \hat{\boldsymbol{k}}\}$ as

$$\hat{\boldsymbol{r}} = \sin\alpha_n\, \cos\delta_n\, \hat{\boldsymbol{\imath}} + \sin\alpha_n\, \sin\delta_n\, \hat{\boldsymbol{\jmath}} + \cos\alpha_n \hat{\boldsymbol{k}} \tag{12}$$

where $\delta_n \in [0,\, 2\pi]\,\mathrm{rad}$ is the clock angle, measured counterclockwise from the direction of $\hat{\boldsymbol{\imath}}$, between the x-axis and the projection of $\hat{\boldsymbol{r}}$ on the plane (x, y), while $\alpha_n \in [0,\, \pi]\,\mathrm{rad}$ is the sail pitch angle, defined as the angle between $\hat{\boldsymbol{r}}$ and $\hat{\boldsymbol{k}} \equiv \hat{\boldsymbol{n}}$, viz.

$$\alpha_n \triangleq \arccos(\hat{\boldsymbol{r}} \cdot \hat{\boldsymbol{k}}) \tag{13}$$

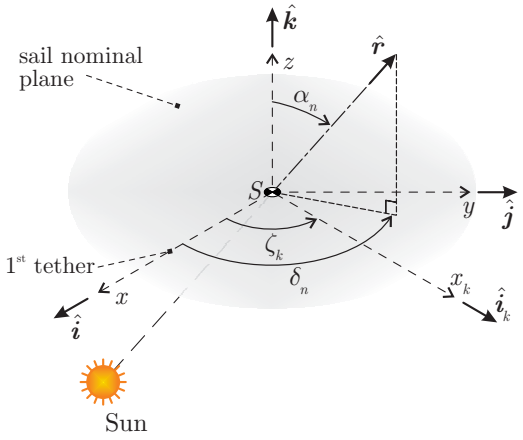

Figure 5: Sail pitch angle α_n.

Taking into account Eqs. (6) and (12), the dot product $\hat{\boldsymbol{r}} \cdot \hat{\boldsymbol{s}}_k$ in Eq. (11) becomes

$$\hat{\boldsymbol{r}} \cdot \hat{\boldsymbol{s}}_k = \frac{\hat{\boldsymbol{r}} \cdot \hat{\boldsymbol{\imath}}_k + f'_k\, \hat{\boldsymbol{r}} \cdot \hat{\boldsymbol{k}}}{\sqrt{1 + (f'_k)^2}} = \frac{\cos(\delta_n - \zeta_k)\, \sin\alpha_n + f'_k\, \cos\alpha_n}{\sqrt{1 + (f'_k)^2}} \tag{14}$$

Therefore, with the aid of Eqs. (6), (11) and (14), the thrust $\mathrm{d}\boldsymbol{F}_{s_k}$ given by Eq. (9) can be rewritten as

$$\mathrm{d}\boldsymbol{F}_{s_k} = \sigma_k\, u\, \mathrm{d}s_k \left[\hat{\boldsymbol{r}} - \frac{\cos(\delta_n - \zeta_k)\, \sin\alpha_n + f'_k\, \cos\alpha_n}{1 + (f'_k)^2} \left(\cos\zeta_k\, \hat{\boldsymbol{\imath}} + \sin\zeta_k\, \hat{\boldsymbol{\jmath}} + f'_k\, \hat{\boldsymbol{k}}\right)\right] \tag{15}$$

Substituting Eqs. (8) and (15) into Eq. (7), and bearing in mind Eq. (4), the compact form of the total force $\mathrm{d}\boldsymbol{F}_k$ acting on the infinitesimal arc-length $\mathrm{d}s_k$ of the generic tether is

$$\mathrm{d}\boldsymbol{F}_k = \mathrm{d}\mathcal{A}_k\, \hat{\boldsymbol{r}} + \mathrm{d}\mathcal{B}_k\, \hat{\boldsymbol{\imath}} + \mathrm{d}\mathcal{C}_k\, \hat{\boldsymbol{\jmath}} + \mathrm{d}\mathcal{D}_k\, \hat{\boldsymbol{k}} \tag{16}$$

where

$$\mathrm{d}\mathcal{A}_k \triangleq \sigma_k\, u \sqrt{1 + (f'_k)^2}\, \mathrm{d}x_k \tag{17}$$

$$\mathrm{d}\mathcal{B}_k \triangleq \left(\rho\, x_k\, \omega^2 - \sigma_k\, u\, \frac{\cos(\delta_n - \zeta_k)\, \sin\alpha_n + f'_k\, \cos\alpha_n}{1 + (f'_k)^2}\right) \cos\zeta_k \sqrt{1 + (f'_k)^2}\, \mathrm{d}x_k \tag{18}$$

$$\mathrm{d}\mathcal{C}_k \triangleq \left(\rho\, x_k\, \omega^2 - \sigma_k\, u\, \frac{\cos(\delta_n - \zeta_k)\, \sin\alpha_n + f'_k\, \cos\alpha_n}{1 + (f'_k)^2}\right) \sin\zeta_k \sqrt{1 + (f'_k)^2}\, \mathrm{d}x_k \tag{19}$$

$$\mathrm{d}\mathcal{D}_k \triangleq -\sigma_k\, u\, f'_k\, \frac{\cos(\delta_n - \zeta_k)\, \sin\alpha_n + f'_k\, \cos\alpha_n}{\sqrt{1 + (f'_k)^2}}\, \mathrm{d}x_k \tag{20}$$

Note that such a decomposition is not unique. Finally, the force $\boldsymbol{F}_k$ acting on the conducting tether is

$$\boldsymbol{F}_k = \int_{x_{r_k}}^{x_{t_k}} \mathrm{d}\boldsymbol{F}_k = \mathcal{A}_k\,\hat{\boldsymbol{r}} + \mathcal{B}_k\,\hat{\boldsymbol{i}} + \mathcal{C}_k\,\hat{\boldsymbol{j}} + \mathcal{D}_k\,\hat{\boldsymbol{k}} \tag{21}$$

with

$$\mathcal{A}_k = \int_{x_{r_k}}^{x_{t_k}} \mathrm{d}\mathcal{A}_k \quad , \quad \mathcal{B}_k = \int_{x_{r_k}}^{x_{t_k}} \mathrm{d}\mathcal{B}_k \quad , \quad \mathcal{C}_k = \int_{x_{r_k}}^{x_{t_k}} \mathrm{d}\mathcal{C}_k \quad , \quad \mathcal{D}_k = \int_{x_{r_k}}^{x_{t_k}} \mathrm{d}\mathcal{D}_k \tag{22}$$

whereas the total force $\boldsymbol{F}$ acting on the E-sail (composed of $N \geq 2$ tethers) is given by

$$\boldsymbol{F} = \sum_{k=0}^{N-1} \boldsymbol{F}_k \equiv \mathcal{A}\,\hat{\boldsymbol{r}} + \mathcal{B}\,\hat{\boldsymbol{i}} + \mathcal{C}\,\hat{\boldsymbol{j}} + \mathcal{D}\,\hat{\boldsymbol{k}} \tag{23}$$

where

$$\mathcal{A} \triangleq \sum_{k=0}^{N-1} \mathcal{A}_k \quad , \quad \mathcal{B} \triangleq \sum_{k=0}^{N-1} \mathcal{B}_k \quad , \quad \mathcal{C} \triangleq \sum_{k=0}^{N-1} \mathcal{C}_k \quad , \quad \mathcal{D} \triangleq \sum_{k=0}^{N-1} \mathcal{D}_k \tag{24}$$

2.3. Propulsive torque

The torque $\mathrm{d}\boldsymbol{T}_k$ given by an infinitesimal arc-length $\mathrm{d}s_k$ of the generic tether is

$$\mathrm{d}\boldsymbol{T}_k = \boldsymbol{d}_k \times \mathrm{d}\boldsymbol{F}_k \tag{25}$$

where the symbol $\times$ denotes the cross product. Taking into account the expressions of $\boldsymbol{d}_k$ and $\mathrm{d}\boldsymbol{F}_k$ given by Eqs. (3) and (16), respectively, and using Eq. (12), $\mathrm{d}\boldsymbol{T}_k$ may be written in a compact form, as a function of $\{\hat{\boldsymbol{i}}, \hat{\boldsymbol{j}}, \hat{\boldsymbol{k}}\}$, as

$$\mathrm{d}\boldsymbol{T}_k = \mathrm{d}\mathcal{E}_k\,\hat{\boldsymbol{i}} + \mathrm{d}\mathcal{F}_k\,\hat{\boldsymbol{j}} + \mathrm{d}\mathcal{G}_k\,\hat{\boldsymbol{k}} \tag{26}$$

where

$$\mathrm{d}\mathcal{E}_k \triangleq \left\{ x_k\,\sin\zeta_k \left[\sigma_k\,u\,\cos\alpha_n - \frac{f'_k\,\sigma_k\,u\,(\sin\alpha_n\,\cos(\delta_n-\zeta_k) + f'_k\,\cos\alpha_n)}{1+(f'_k)^2} \right] + \right.$$

$$\left. - f_k\,\sin\zeta_k \left[\rho\,x_k\,\omega^2 - \frac{\sigma_k\,u\,(\sin\alpha_n\,\cos(\delta_n-\zeta_k) + f'_k\,\cos\alpha_n)}{1+(f'_k)^2} \right] - f_k\,\sigma_k\,u\,\sin\alpha_n\,\sin\delta_n \right\} \sqrt{1+(f'_k)^2}\,\mathrm{d}x_k \tag{27}$$

$$\mathrm{d}\mathcal{F}_k \triangleq \left\{ -x_k\,\cos\zeta_k \left[\sigma_k\,u\,\cos\alpha_n - \frac{f'_k\,\sigma_k\,u\,(\sin\alpha_n\,\cos(\delta_n-\zeta_k) + f'_k\,\cos\alpha_n)}{1+(f'_k)^2} \right] + \right.$$

$$\left. + f_k\,\cos\zeta_k \left[\rho\,x_k\,\omega^2 - \frac{\sigma_k\,u\,(\sin\alpha_n\,\cos(\delta_n-\zeta_k) + f'_k\,\cos\alpha_n)}{1+(f'_k)^2} \right] + f_k\,\sigma_k\,u\,\sin\alpha_n\,\cos\delta_n \right\} \sqrt{1+(f'_k)^2}\,\mathrm{d}x_k \tag{28}$$

$$\mathrm{d}\mathcal{G}_k \triangleq \sigma_k\,u\,x_k\,\sin\alpha_n\,\sin(\delta_n-\zeta_k)\,\sqrt{1+(f'_k)^2}\,\mathrm{d}x_k \tag{29}$$

The torque $\boldsymbol{T}_k$ acting on the generic tether is

$$\boldsymbol{T}_k = \int_{x_{r_k}}^{x_{t_k}} \mathrm{d}\boldsymbol{T}_k = \mathcal{E}_k\,\hat{\boldsymbol{i}} + \mathcal{F}_k\,\hat{\boldsymbol{j}} + \mathcal{G}_k\,\hat{\boldsymbol{k}} \tag{30}$$

with

$$\mathcal{E}_k = \int_{x_{r_k}}^{x_{t_k}} \mathrm{d}\mathcal{E}_k \quad , \quad \mathcal{F}_k = \int_{x_{r_k}}^{x_{t_k}} \mathrm{d}\mathcal{F}_k \quad , \quad \mathcal{G}_k = \int_{x_{r_k}}^{x_{t_k}} \mathrm{d}\mathcal{G}_k \tag{31}$$

whereas the total torque $\boldsymbol{T}$ acting on the E-sail is

$$\boldsymbol{T} = \sum_{k=0}^{N-1} \boldsymbol{T}_k \equiv \mathcal{E}\,\hat{\boldsymbol{i}} + \mathcal{F}\,\hat{\boldsymbol{j}} + \mathcal{G}\,\hat{\boldsymbol{k}} \tag{32}$$

where

$$\mathcal{E} \triangleq \sum_{k=0}^{N-1} \mathcal{E}_k \quad , \quad \mathcal{F} \triangleq \sum_{k=0}^{N-1} \mathcal{F}_k \quad , \quad \mathcal{G} \triangleq \sum_{k=0}^{N-1} \mathcal{G}_k \tag{33}$$

Equations (21) and (32) are the expressions of the total force and torque acting on the E-sail with a given tether shape, length, and angular separation between tethers. However, some simplifying assumptions need to be introduced to get a more tractable form of both $\boldsymbol{F}$ and $\boldsymbol{T}$, as is thoroughly discussed in the next section.

3. Case of a Sun-facing E-sail

The previous general results are now specialized to the noteworthy case of a Sun-facing E-sail [21, 22], which corresponds to when the spacecraft spin axis z coincides with the Sun-spacecraft line (i.e., $\hat{\boldsymbol{k}} \equiv \hat{\boldsymbol{r}}$). In this case the pitch angle α_n is zero by construction, whereas δ_n can be set to zero without loss of generality, because $\hat{\boldsymbol{r}}$ is orthogonal to the plane (x, y), viz.

$$\alpha_n = 0 \quad , \quad \delta_n = 0 \tag{34}$$

Assuming all tethers to have the same length L and the same voltage V_k (that is, the same value of σ_k, see Eq. (10)), the E-sail may reasonably be assumed to have a cylindrical symmetry around the z-axis. The notation can be therefore simplified by dropping the subscript k in the variables $\{x_k,\, f_k,\, x_{r_k},\, x_{t_k},\, \sigma_k\}$. Accordingly, all tethers have the same shape (i.e., they are described via the same mathematical function $f = f(x)$), and are arranged at the same angle apart from each other, viz.

$$\zeta_k = \frac{2\pi}{N}\, k \tag{35}$$

with $k = 0, 1, \ldots, (N-1)$.

Taking into account Eqs. (34)–(35), and bearing in mind that $\hat{\boldsymbol{k}} \equiv \hat{\boldsymbol{r}}$, from Eq. (23) the total force $\boldsymbol{F}$ becomes

$$\begin{aligned} \boldsymbol{F} = &\left(\sigma\, u\, N \int_{x_r}^{x_t} \frac{1}{\sqrt{1+(f')^2}}\, \mathrm{d}x \right) \hat{\boldsymbol{r}} + \\ &+ \left(\rho\, \omega^2 \int_{x_r}^{x_t} x\, \sqrt{1+(f')^2}\, \mathrm{d}x - \sigma\, u \int_{x_r}^{x_t} \frac{f'}{\sqrt{1+(f')^2}}\, \mathrm{d}x \right) \left[\hat{\boldsymbol{i}} \sum_{k=0}^{N-1} \cos\left(\frac{2\pi}{N}\, k\right) + \hat{\boldsymbol{j}} \sum_{k=0}^{N-1} \sin\left(\frac{2\pi}{N}\, k\right) \right] \end{aligned} \tag{36}$$

and the total torque (32) is

$$\begin{aligned} \boldsymbol{T} = &\hat{\boldsymbol{i}} \left[\int_{x_r}^{x_t} \frac{\sigma\, u\, x - \rho\, \omega^2\, x\, f\, [1+(f')^2] + \sigma\, u\, f\, f'}{\sqrt{1+(f')^2}}\, \mathrm{d}x \right] \sum_{k=0}^{N-1} \sin\left(\frac{2\pi}{N}\, k\right) + \\ &- \hat{\boldsymbol{j}} \left[\int_{x_r}^{x_t} \frac{\sigma\, u\, x - \rho\, \omega^2\, x\, f\, [1+(f')^2] + \sigma\, u\, f\, f'}{\sqrt{1+(f')^2}}\, \mathrm{d}x \right] \sum_{k=0}^{N-1} \cos\left(\frac{2\pi}{N}\, k\right) \end{aligned} \tag{37}$$

whereas the single tether length L can be written, as a function of $\{x_r,\, x_t,\, f'\}$, as

$$L = \int_{x_r}^{x_t} \sqrt{1+(f')^2}\, \mathrm{d}x \tag{38}$$

According to Ref. [20], when $N \geq 2$ the summations in Eqs. (36)-(37) are

$$\sum_{k=0}^{N-1} \sin\left(\frac{2\pi}{N}\,k\right) = \sum_{k=0}^{N-1} \cos\left(\frac{2\pi}{N}\,k\right) = 0 \tag{39}$$

and the final form of the total force and torque given by a Sun-facing E-sail reduces to

$$\boldsymbol{F} = \left(\sigma\, u\, N \int_{x_r}^{x_t} \frac{1}{\sqrt{1+(f')^2}}\,\mathrm{d}x\right)\hat{\boldsymbol{r}} \qquad , \qquad \boldsymbol{T} = 0 \tag{40}$$

Note that the result $\boldsymbol{T} = 0$ is consistent with the assumption of an E-sail with cylindrical symmetry with respect to the spin axis, whereas the actual expression of the total force $\boldsymbol{F}$ (that is, the E-sail propulsive thrust) depends on the tether shape via the analytical function $f' = \mathrm{d}f/\mathrm{d}x$. Some noteworthy cases are now discussed to better investigate the impact of the tether shape $f = f(x)$ on the E-sail total force $\boldsymbol{F}$.

3.1. Flat shape

When all the tethers are arranged on a flat surface that, in this case, coincides with the E-sail nominal plane, the condition $f' = 0$ is to be enforced in the first of Eqs. (40). The total force becomes

$$\boldsymbol{F} = \sigma\, u\, N\, L\, \hat{\boldsymbol{r}} \tag{41}$$

where $L = (x_t - x_r)$, see Eq. (38). In particular, Eq. (41) is consistent with the result discussed in Ref. [20] for a Sun-facing E-sail (i.e., when $\alpha_n = 0$).

Actually, the case of a purely flat E-sail is only a first approximation of the real sail shape. In fact, all tethers tend to move away from the E-sail nominal plane (x, y) and to take a three-dimensional arrangement, while keeping, according to the previous assumptions, a cylindrical symmetry.

3.2. Conic shape

An interesting approximation of the actual E-sail three-dimensional arrangement is given by a conic shape. In that case, each tether may be analytically described as

$$f(x) = b_c\, x_r \left(\frac{x}{x_r} - 1\right) \qquad \text{with} \qquad x \in [x_r,\, x_t] \tag{42}$$

where $b_c > 0$ is a (constant) dimensionless coefficient, whose value depends on the aperture angle β of the right circular cone that approximates the E-sail shape through the formula

$$\beta = \pi - 2\,\arctan(b_c) \tag{43}$$

Since $f'(x) = b_c$, from the first of Eqs. (40) the total force results

$$\boldsymbol{F} = \frac{\sigma\, u\, N\, L}{\sqrt{1+b_c^2}}\,\hat{\boldsymbol{r}} \tag{44}$$

where $L = (x_t - x_r)\,\sqrt{1+b_c^2}$ is the tether length. Equation (44) is similar to Eq. (41), where a sort of "effective" tether length (equal to $L/\sqrt{1+b_c^2}$) is considered in place of the actual length. Note that $L/\sqrt{1+b_c^2}$ is the tether length when projected on the E-sail nominal plane (x, y).

3.3. Parabolic shape

A simple way to take the tether curvature into account is to consider a parabolic shape. Each tether is modelled as

$$f(x) = b_p\, x_r \left(\frac{x}{x_r} - 1\right)^2 \qquad \text{with} \qquad x \in [x_r,\, x_t] \tag{45}$$

where the (constant) dimensionless coefficient $b_p > 0$ depends on the tether curvature. In this case

$$f'(x) = 2\,b_p\,\left(\frac{x}{x_r} - 1\right) \tag{46}$$

and, bearing in mind the first of Eqs. (40), the total force becomes

$$\boldsymbol{F} = \sigma\,u\,N\,\frac{x_r}{2\,b_p}\,\mathrm{arcsinh}\left[2\,b_p\,\left(\frac{x_t}{x_r} - 1\right)\right]\,\hat{\boldsymbol{r}} \tag{47}$$

where $\{x_r,\, x_t,\, b_p\}$ are related to the tether length L according to

$$L = \frac{x_r}{4\,b_p}\,\mathrm{arcsinh}\left[2\,b_p\,\left(\frac{x_t}{x_r} - 1\right)\right] + b_p\,x_r\,\left(\frac{x_t}{x_r} - 1\right)\,\sqrt{\left(\frac{x_t}{x_r} - 1\right)^2 + \frac{1}{4\,b_p^2}} \tag{48}$$

3.4. Logarithmic shape

An interesting case is obtained when the tether shape $f(x)$ is described through a logarithmic function of the distance x. Indeed, as will be shown in the next section, the tether equilibrium shape of a Sun-facing E-sail under the action of the external forces just follows a logarithmic function provided the spin rate ω is sufficiently large.

Therefore, let the shape function be

$$f(x) = b_l\,x_t\,\ln\left(\frac{x + x_t}{x_r + x_t}\right) \qquad \text{with} \qquad x \in [x_r,\, x_t] \tag{49}$$

from which

$$f'(x) = \frac{b_l}{1 + \dfrac{x}{x_t}} \tag{50}$$

where the dimensionless coefficient $b_l > 0$ is a given parameter. Substituting Eq. (50) into the first of Eqs. (40), the resultant force vector becomes

$$\boldsymbol{F} = \sigma\,u\,N\,x_t\,\left[\sqrt{4 + b_l^2} - \sqrt{b_l^2 + (x_r/x_t + 1)^2}\right]\,\hat{\boldsymbol{r}} \tag{51}$$

where $\{x_r,\, x_t,\, b_l\}$ are related to the tether length L through the equation

$$L = x_t\,\left[\sqrt{4 + b_l^2} - b_l\,\mathrm{arcsinh}\left(\frac{b_l}{2}\right) - \sqrt{b_l^2 + (x_r/x_t + 1)^2} + b_l\,\mathrm{arcsinh}\left(\frac{b_l}{x_r/x_t + 1}\right)\right] \tag{52}$$

The expression (51) is very useful from a practical viewpoint, as is now thoroughly discussed.

4. Tether equilibrium shape of a Sun-facing E-sail

The analytical, approximate, equilibrium shape of a generic tether of a Sun-facing E-sail can be obtained using the approach discussed in Ref. [8]. Assuming a rotating E-sail, Toivanen and Janhunen [8] describe the equilibrium tether shape with an integral equation, which is solved numerically. In particular, using an analytical approximation of the tether shape, Toivanen and Janhunen [8] also obtain closed-form expressions for both the thrust and torque arising from the solar wind momentum transfer to the E-sail. Their results essentially state that the tethers form a cone near the spacecraft, while they are (substantially) flattened around the tip region by the centrifugal force. Note that Toivanen and Janhunen [8] consider a mass at the tether tip (that is, a mass that models the presence of a remote unit), whereas this work considers the tether only, without any tip mass.

It will be shown now that the exact tether slope at the tip can be found analytically. An accurate approximation of the tether equilibrium shape can also be obtained, using the model discussed in the last

section. To that end, enforcing the Sun-facing conditions $\alpha_n = 0$ and $\delta_n = 0$ into Eqs. (16)–(20), the total force $\mathrm{d}\boldsymbol{F}_k$ acting on the infinitesimal arc-length $\mathrm{d}s_k$ becomes

$$\mathrm{d}\boldsymbol{F}_k = \left[\left(\frac{\rho\,\omega^2\,x_k}{\sigma_k\,u} - \frac{f_k'}{1+(f_k')^2} \right) \hat{\boldsymbol{\imath}}_k + \frac{1}{1+(f_k')^2}\,\hat{\boldsymbol{k}} \right] \sigma_k\,u\,\sqrt{1+(f_k')^2}\,\mathrm{d}x_k \tag{53}$$

where $\hat{\boldsymbol{\imath}}_k$, given by Eq. (2), is the unit vector obtained from the projection of $\mathrm{d}\boldsymbol{F}_k$ on the E-sail nominal plane (x, y).

Without loss of generality, the notation may be simplified by dropping the subscript k in the variables $\{x_k,\, f_k',\, \sigma_k,\, \hat{\boldsymbol{\imath}}_k\}$ of Eq. (53). Assume the generic tether to have no bending stiffness, so that only an internal tension acts tangential to its neutral axis. In this case, according to Toivanen and Janhunen [8], the direction of the vector tangent to the tether at the generic point P of abscissa $x \in [x_r,\, x_t]$ is parallel to the direction of the integral of $\mathrm{d}\boldsymbol{F}$ from x to x_t (i.e., the integral of the total force from P to the tether tip). Therefore, from Eq. (53), the tether slope f' at point P is the solution of the following integro-differential equation

$$f'(x) = \frac{\sigma\,u \displaystyle\int_x^{x_t} \frac{\mathrm{d}y}{\sqrt{1+(f')^2}}}{\rho\,\omega^2 \displaystyle\int_x^{x_t} y\,\sqrt{1+(f')^2}\,\mathrm{d}y - \sigma\,u \int_x^{x_t} \frac{f'\,\mathrm{d}y}{\sqrt{1+(f')^2}}} \tag{54}$$

where the numerator (denominator) in the right-hand side is the component along the z-axis (x-axis) of the resultant force acting on the tether arc between P and the tip, that is

$$F_x(x) \triangleq \rho\,\omega^2 \int_x^{x_t} y\,\sqrt{1+(f')^2}\,\mathrm{d}y - \sigma\,u \int_x^{x_t} \frac{f'\,\mathrm{d}y}{\sqrt{1+(f')^2}} \tag{55}$$

$$F_z(x) \triangleq \sigma\,u \int_x^{x_t} \frac{\mathrm{d}y}{\sqrt{1+(f')^2}} \tag{56}$$

Introduce the dimensionless abscissa $h \triangleq x/x_t$, with $h \in [h_r,\, 1]$, where $h_r \triangleq x_r/x_t \geq 0$ is the value at the root section. Equation (54) can be conveniently rewritten as

$$f'(h) = \frac{\displaystyle\int_h^1 \frac{\mathrm{d}y}{\sqrt{1+(f')^2}}}{K \displaystyle\int_h^1 y\,\sqrt{1+(f')^2}\,\mathrm{d}y - \int_h^1 \frac{f'\,\mathrm{d}y}{\sqrt{1+(f')^2}}} \tag{57}$$

where $K > 0$ is a dimensionless "shaping parameter" defined as

$$K \triangleq \frac{\rho\,\omega^2\,x_t}{\sigma\,u} \tag{58}$$

which relates the tether equilibrium shape of a Sun-facing E-sail to the ratio of electric ($\sigma\,u$) to centrifugal ($\rho\,\omega^2\,x_t$) effects.

The tether slope at the tip, that is, the exact value of $f'(h=1) \triangleq f_t'$ can be obtained from Eq. (57) using a limit procedure, viz.

$$f_t' = \lim_{h\to 1} f'(h) = \frac{1}{K\,[1+(f_t')^2] - f_t'} \tag{59}$$

which can be rewritten as

$$\left(f_t' - \frac{1}{K} \right)\,\left[(f_t')^2 + 1 \right] = 0 \tag{60}$$

whose only real solution is

$$f_t' = \frac{1}{K} \equiv \frac{\sigma\, u}{\rho\, \omega^2\, x_t} \tag{61}$$

As expected, the tether slope at the tip sharply reduces as the E-sail spin rate increases. The variation of f_t' with $\{x_t,\, \omega\}$, when $\sigma = 9.3 \times 10^{-13}\,\mathrm{kg/m/s}$, $\rho = 10^{-5}\,\mathrm{kg/m}$ and $u = 400\,\mathrm{km/s}$, is shown in Fig. 6. In particular, $f_t' \leq 0.1$ (or $K \geq 10$) when $\omega \geq 5\,\mathrm{rph}$ and $x_t \geq 5\,\mathrm{km}$, which implies a tether slope at the tip less than 6 deg. Having obtained the exact value of f_t', it is now possible to calculate the function $f'(x)$ (or $f'(h)$).

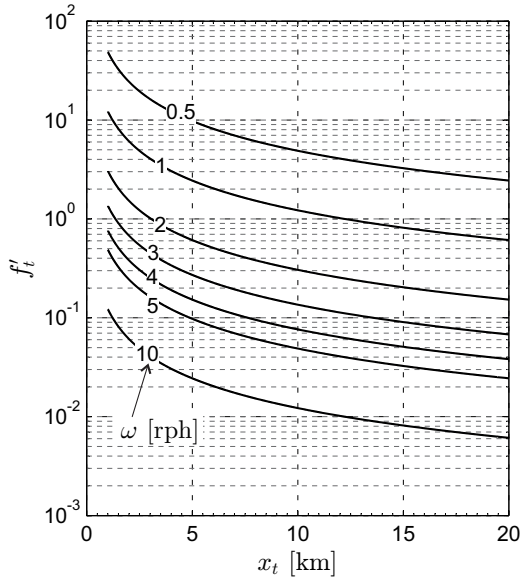

Figure 6: Tip slope f_t' as a function of the spin rate ω and the spin axis-tip distance x_t, see Eq. (61).

To that end a recursive procedure is necessary, which, starting from the tether tip and backward proceeding toward the root, numerically solves Eq. (57) for a given value of K. The results of such a procedure are summarized in Fig. 7 for some values of the shaping parameter K. The figure shows that $f_t' = 1/K$, in agreement with Eq. (61). Also note that in the ideal case $h_r = 0$, which amounts neglecting the main body width and assuming the tether to be attached to the z-axis, the tether slope at root is $f'(0) \simeq 2\, f_t' \equiv 2/K$ when the shaping parameter is sufficiently large, that is, when $K \geq 5$. In that case $1/K \leq f' \leq 2/K$, or

$$\frac{K^2+1}{K^2} \leq 1 + (f')^2 \leq \frac{K^2+4}{K^2} \tag{62}$$

which implies

$$1 + (f')^2 \simeq 1 \tag{63}$$

The tether shape may be obtained by means of a numerical integration, and the results are summarized in Fig. 8 assuming $h_r = 0$. Notably, an accurate analytical approximation may also be obtained, as is discussed in the next section.

4.1. Tether shape analytical approximation

An accurate analytical approximation of the tether shape can be obtained for a sufficiently large value of the shaping parameter, for example when $K \geq 5$. In that case, substituting Eq. (63) into Eq. (57), the result is

$$f'(h) \simeq \frac{\displaystyle\int_h^1 \mathrm{d}y}{\displaystyle K \int_h^1 y\ \mathrm{d}y - \int_h^1 f'\,\mathrm{d}y} = \frac{2\,(1-h)/K}{\displaystyle 1 - h^2 - 2\,\frac{[f_t - f(h)]}{K\, x_t}} \tag{64}$$

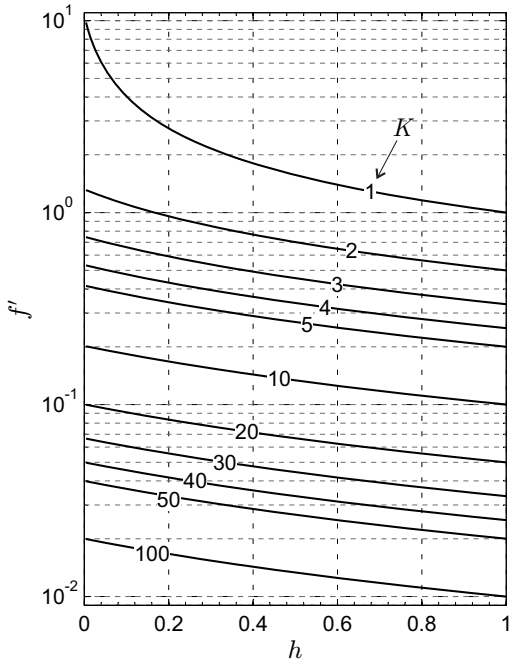

Figure 7: Tether slope f' as a function of the dimensionless abscissa $h = x/x_t$ and the shaping parameter K, see Eq. (58).

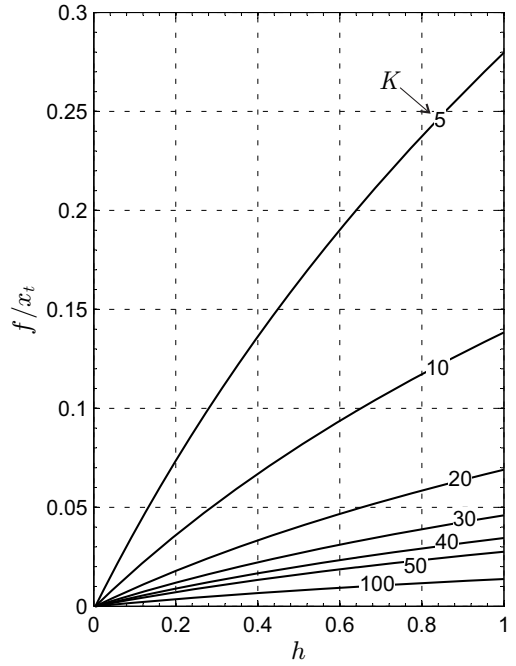

Figure 8: Tether shape as a function of $h = x/x_t$ and K obtained through numerical integration.

Since $\max\{2\ [f_t - f(h)]/(K\,x_t)\} \simeq 0.11$, see Fig. 8, the last relation may be further simplified as

$$f'(h) \simeq \frac{2}{K\ (1+h)} \tag{65}$$

Notably, the approximation of Eq. (65) gives the exact value at tether tip, $f'_t = 1/K$, and also it captures the approximate value at tether root, $f'(0) = 2/K$, in agreement with the estimate obtained in the last section.

Figure 9 compares the analytic approximation given by Eq. (65) (dash line) with the numerical solution (solid line) and shows that the two results are nearly coincident when $K \geq 5$. Accordingly, an accurate

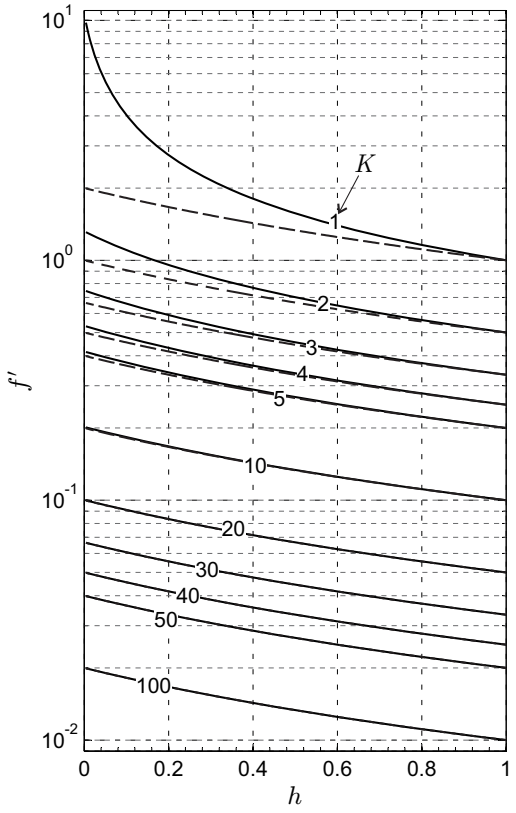

Figure 9: Tether slope f' as a function of h and K: numerical (solid line) vs. analytical approximation (dash line).

analytical solution of the tether shape can be found from Eq. (65). Indeed, using a variable separation and integrating both sides, it may be verified that

$$f(h) = \frac{2\,x_t}{K}\,\ln\left(\frac{1+h}{1+h_r}\right) \qquad \text{with} \qquad h \in [h_r,\,1] \tag{66}$$

or, using Eq. (58)

$$f(x) = \frac{2\,\sigma\,u}{\rho\,\omega^2}\,\ln\left(\frac{x+x_t}{x_r+x_t}\right) \qquad \text{with} \qquad x \in [x_r,\,x_t] \tag{67}$$

The latter coincides with Eq. (49) when

$$b_l = \frac{2\,\sigma\,u}{\rho\,\omega^2\,x_t} \equiv \frac{2}{K} \tag{68}$$

Equation (67) proofs the importance of a logarithmic shape for describing the equilibrium configuration of a Sun-facing E-sail. Its actual accuracy is better appreciated with the aid of Fig. 10, which plots Eq. (66) with $h_r = 0.01$. The obtained results are nearly coincident with those reported in Fig. 8, which correspond to a numerical integration of the actual tether slope.

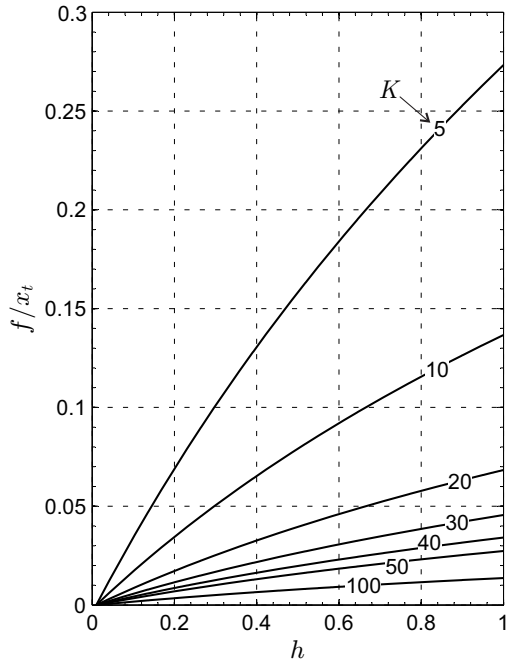

Figure 10: Tether approximate shape as a function of the dimensionless abscissa $h = x/x_t$ and K when $h_r = 0.01$, see Eq. (66).

5. Tether root force

Due to the E-sail rotation, each tether experiences a tension force τ with a maximum value τ_r, which occurs at the root section, that is, when $x = x_r$ (or $h = h_r$). The value of τ_r is obtained by imposing the equilibrium condition of all forces acting on the tether at the root, that is $\tau_r = \sqrt{F_{x_r}^2 + F_{z_r}^2}$, where $F_{x_r} \triangleq F_x(x_r)$ and $F_{z_r} \triangleq F_z(x_r)$, see Eqs. (55)-(56). The tension at the root section is therefore

$$\tau_r = \frac{\sqrt{1 + (f_r')^2}}{f_r'} F_{z_r} \tag{69}$$

where

$$F_{z_r} = \sigma\, u \int_{x_r}^{x_t} \frac{\mathrm{d}y}{\sqrt{1 + (f')^2}} \tag{70}$$

and $f_r' \equiv f'(x_r) = F_{z_r}/F_{x_r}$ is the tether slope at the root section. Equation (69) can be rewritten in a dimensionless form as

$$\frac{\tau_r}{\sigma\, u\, x_t} = \frac{\sqrt{1 + (f_r')^2}}{f_r'} \int_{h_r}^{1} \frac{\mathrm{d}y}{\sqrt{1 + (f')^2}} \tag{71}$$

whose numerical solution is obtained, for a given value of K, using the function $f' = f'(h)$ calculated through the iterative procedure described in the last section. For example, assuming $h_r = 0$, the dimensionless value of τ_r is shown in Fig. 11 as a function of K. Note that $\tau_r/(\sigma\, u\, x_t)$ has a nearly linear variation with K, with an angular coefficient equal to $1/2$. This same result will now be confirmed by an analytical approximation.

5.1. Analytical approximation of τ_r

Assuming a shaping parameter $K \geq 5$, the tether slope is well approximated by Eq. (65), therefore

$$\int_{h_r}^{1} \frac{\mathrm{d}y}{\sqrt{1 + (f')^2}} = \frac{2\sqrt{K^2 + 1} - \sqrt{K^2 (1 + h_r)^2 + 4}}{K} \tag{72}$$

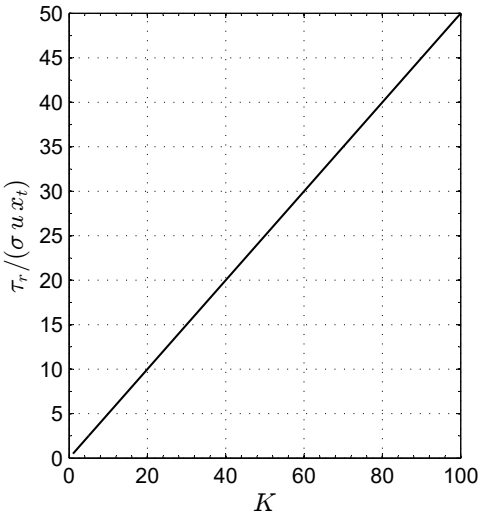

Figure 11: Dimensionless tension at tether root as a function of K when $h_r = 0$, see Eq. (66).

Substituting this last relation into Eq. (71) in which $f_r' \simeq 2/K/(1+h_r)$, the result is

$$\frac{\tau_r}{\sigma\, u\, x_t} = \frac{\sqrt{K^2\,(1+h_r)^2+4}}{2\,K}\left[2\,\sqrt{K^2+1}-\sqrt{K^2\,(1+h_r)^2+4}\right] \tag{73}$$

In the limit as $h_r \to 0$, the last relation may be further simplified taking into account that $K^2 \gg 1$. The compact and elegant solution is

$$\frac{\tau_r}{\sigma\, u\, x_t} = \frac{K}{2} \equiv \frac{\rho\,\omega^2\, x_t}{2\,\sigma\, u} \tag{74}$$

which is in agreement with the plot shown in Fig. 11. This last relation allows the value of τ_r to be related with the tether length L, when its equilibrium shape is a logarithmic function. In fact, assuming $x_r = 0$ and substituting Eq. (74) into Eq. (68) and then into Eq. (52), it may be verified that

$$\frac{L}{x_t} = \sqrt{4+\left(\frac{\sigma\, u\, x_t}{\tau_r}\right)^2}-\sqrt{1+\left(\frac{\sigma\, u\, x_t}{\tau_r}\right)^2}+\left(\frac{\sigma\, u\, x_t}{\tau_r}\right)\left[\operatorname{arcsinh}\left(\frac{\sigma\, u\, x_t}{\tau_r}\right)-\operatorname{arcsinh}\left(\frac{\sigma\, u\, x_t}{2\,\tau_r}\right)\right] \tag{75}$$

which is drawn in Fig. 12 when $K \in [5,\, 100]$. The tension at the root can be expressed as a function of the pair of design parameters $\{\omega,\, L\}$ by combining Eqs. (74) and (75). Its maximum value cannot exceed the tether yield strength, which is about 0.1275 N for a μm-diameter aluminum tether, with a linear mass density ρ approximately equal to 10 grams per kilometer [23].

For example, assuming $V = 20\,\text{kV}$ [23], Fig. 13 shows how the tension τ_r varies with the tether length L and spin rate ω when $x_r = 0$. Note that each level curve breaks down when the yield strength $\tau_{\max}$ is achieved (i.e., when $\tau_r = \tau_{\max}$). According to Fig. 13, the tension τ_r roughly exhibits a parabolic behaviour with the spacecraft spin rate ω for a given value of L. In particular, the figure shows that the maximum allowable spin rate for a baseline tether length of 20 km is about $\omega = 4.57\,\text{rph}$, whereas the value of x_t is 19.983 km. In this case, $K \simeq 34$ and the dimensionless root tether is $\tau_{\max}/(\sigma\, u\, x_t) \simeq 17$, in agreement with the numerical results shown in Fig. 11.

6. Conclusions

The thrust and torque vectors provided by a spinning electric solar wind sail of given shape have been calculated in a fully analytical form as a function of the spacecraft attitude. This analysis is based on the hypothesis that each tether is deformed by the external forces such that its shape belongs to a plane

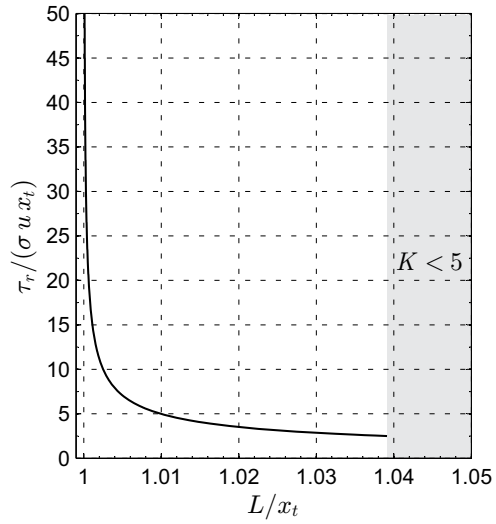

Figure 12: Dimensionless tether tension at root as a function of the dimensionless tether length when $h_r = 0$.

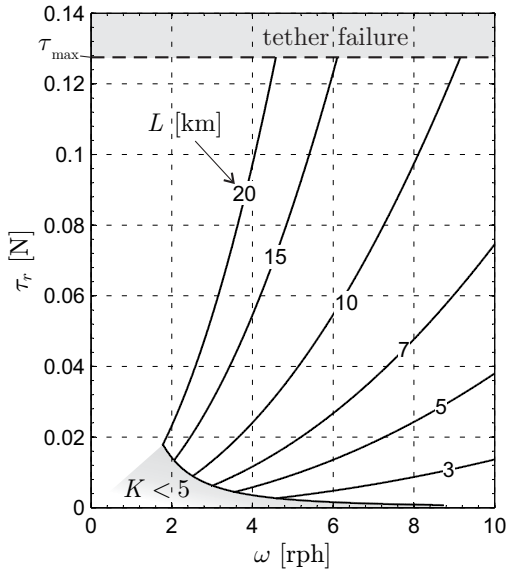

Figure 13: Root tension τ_r as a function of L and ω when $\rho = 10\,\mathrm{g/km}$, $x_r = 0$, and $\tau_{\max} = 0.1275\,\mathrm{N}$. Data adapted from Ref. [23].

passing through the E-sail spin axis. The general expressions of the thrust and torque vectors have been then specialized to the case of a Sun-facing sail, with a tether arrangement assumed to be axially symmetric with respect to the spacecraft spin axis.

The results have been applied to some noteworthy tether shapes, including the flat and the logarithmic cases. In particular, the equilibrium shape of any tether, when the electric sail axis is parallel to the Sun-spacecraft direction, is close to a logarithmic arc, in agreement with the numerical results of the recent literature. The discussed mathematical model allows the geometry of an axially-symmetric Sun-facing sail to be related to the yield strength of the cable. The problem is that the generation of a high thrust level requires the tethers to be maintained stretched, but the spin rate must account for the tether structural load resulting from the centrifugal force.

A natural extension of this work consists in the analysis of the effects of a pitch angle different from zero,

that is, when the sail produces an off-axis thrust. The latter assumption breaks the axial-symmetry condition and, therefore, requires a different approach to analyze the coupling effects between the sail geometry and the spacecraft attitude. In particular, the actual tether shape can only be checked by simulation through a finite element analysis, which is left to future analysis.

Acknowledgement

The authors gratefully acknowledge the constructive comments made by the anonymous reviewers that helped improve the paper.

References

[1] P. Janhunen, Electric sail for spacecraft propulsion, Journal of Propulsion and Power 20 (4) (2004) 763–764, doi: 10.2514/1.8580.

[2] P. Janhunen, A. Sandroos, Simulation study of solar wind push on a charged wire: basis of solar wind electric sail propulsion, Annales Geophysicae 25 (3) (2007) 755–767, doi: 10.5194/angeo-25-755-2007.

[3] P. Janhunen, P. K. Toivanen, J. Polkko, et al., Electric solar wind sail: Toward test missions, Review of Scientific Instruments 81 (11) (2010) 111301–1–11301–11, doi: 10.1063/1.3514548.

[4] P. Janhunen, Photonic spin control for solar wind electric sail, Acta Astronautica 83 (2013) 85–90, doi: 10.1016/j.actaastro.2012.10.017.

[5] P. Janhunen, The electric solar wind sail status report, in: European Planetary Science Congress 2010, Vol. 5, European Planetology Network and the European Geosciences Union, 2010, paper EPSC 2010-297.

[6] P. Toivanen, P. Janhunen, Spin plane control and thrust vectoring of electric solar wind sail, Journal of Propulsion and Power 29 (1) (2013) 178–185, doi: 10.2514/1.B34330.

[7] P. Toivanen, P. Janhunen, J. Envall, Electric sail control mode for amplified transverse thrust, Acta Astronautica 106 (2015) 111–119, doi: 10.1016/j.actaastro.2014.10.031.

[8] P. Toivanen, P. Janhunen, Thrust vectoring of an electric solar wind sail with a realistic sail shape, Acta Astronautica 131 (2017) 145–151, doi: 10.1016/j.actaastro.2016.11.027.

[9] G. Mengali, A. A. Quarta, P. Janhunen, Electric sail performance analysis, Journal of Spacecraft and Rockets 45 (1) (2008) 122–129, doi: 10.2514/1.31769.

[10] A. A. Quarta, G. Mengali, Electric sail mission analysis for outer solar system exploration, Journal of Guidance, Control, and Dynamics 33 (3) (2010) 740–755, doi: 10.2514/1.47006.

[11] L. Niccolai, A. A. Quarta, G. Mengali, Electric sail-based displaced orbits with refined thrust model, Proceedings of the Institution of Mechanical Engineers, Part G: Journal of Aerospace Engineering (in press) , doi: 10.1177/0954410016679195.

[12] L. Niccolai, A. A. Quarta, G. Mengali, Electric sail elliptic displaced orbits with advanced thrust model, Acta Astronautica 138 (2017) 503–511, doi: 10.1016/j.actaastro.2016.10.036.

[13] L. Niccolai, A. A. Quarta, G. Mengali, Two-dimensional heliocentric dynamics approximation of an electric sail with fixed attitude, Aerospace Science and Technology 71 (2017) 441–446, doi: 10.1016/j.ast.2017.09.045.

[14] A. A. Quarta, G. Mengali, Minimum-time trajectories of electric sail with advanced thrust model, Aerospace Science and Technology 55 (2016) 419–430, doi: 10.1016/j.ast.2016.06.020.

[15] A. A. Quarta, G. Mengali, P. Janhunen, Optimal interplanetary rendezvous combining electric sail and high thrust propulsion system, Acta Astronautica 68 (5–6) (2011) 603–621, doi: 10.1016/j.actaastro.2010.01.024.

[16] A. A. Quarta, G. Mengali, Trajectory approximation for low-performance electric sail with constant thrust angle, Journal of Guidance, Control, and Dynamics 36 (3) (2013) 884–887, doi: 10.2514/1.59076.

[17] A. A. Quarta, G. Aliasi, G. Mengali, Electric solar wind sail optimal transit in the circular restricted three body problem, Acta Astronautica 116 (2015) 43–49, doi: 10.1016/j.actaastro.2015.06.017.

[18] A. A. Quarta, G. Mengali, Electric sail missions to potentially hazardous asteroids, Acta Astronautica 66 (9–10) (2010) 1506–1519, doi: 10.1016/j.actaastro.2009.11.021.

[19] G. Mengali, A. A. Quarta, P. Janhunen, Considerations of electric sailcraft trajectory design, Journal of the British Interplanetary Society 61 (8) (2008) 326–329 .

[20] M. Huo, G. Mengali, A. A. Quarta, Electric sail thrust model from a geometrical perspective, Journal of Guidance, Control and Dynamics (in press) , doi: 10.2514/1.G003169.

[21] G. Mengali, A. A. Quarta, G. Aliasi, A graphical approach to electric sail mission design with radial thrust, Acta Astronautica 82 (2) (2013) 197–208, doi: 10.1016/j.actaastro.2012.03.022.

[22] A. A. Quarta, G. Mengali, Analysis of electric sail heliocentric motion under radial thrust, Journal of Guidance, Control and Dynamics 39 (6) (2016) 1431–1435, doi: 10.2514/1.G001632.

[23] H. Seppänen, T. Rauhala, S. Kiprich, J. Ukkonen, M. Simonsson, R. Kurppa, P. Janhunen, E. Hæggstrom, One kilometer (1 km) electric solar wind sail tether produced automatically, Review of Scientific Instruments 84 (9), doi: 10.1063/1.4819795.